The Astrophysical Journal, 738:179 (8pp), 2011 September 10 doi:10.1088/0004-637X/738/2/179

SYMPATHETIC FILAMENT ERUPTIONS CONNECTED BY CORONAL DIMMINGS

Yunchun Jiang, Jiayan Yang, Junchao Hong, Yi Bi, and Ruisheng Zheng
National Astronomical Observatories/Yunnan Astronomical Observatory, Chinese Academy of Sciences,
P.O. Box 110, Kunming 650011, China; jyc@ynao.ac.cn
Received 2010 June 7; accepted 2011 June 25; published 2011 August 24

ABSTRACT

We present for the first time detailed observations of three successive, interdependent filament eruptions that occurred one by one within 5 hr from different locations beyond the range of a single active region. The first eruption was observed from an active region and was associated with a coronal mass ejection (CME), during which diffuse and complex coronal dimmings formed, largely extending to the two other filaments located in quiet-Sun regions. Then, both quiescent filaments consecutively underwent the second and third eruptions, while the nearby dimmings were persistent. Comparing the result of a derived coronal magnetic configuration, the magnetic connectivity between the dimmings suggested that they were caused by the joint effect of simple expansion of overlying loop systems forced by the first eruption, as well as by its erupting field interacting or reconnecting with the surrounding magnetic structures. Note that the dimming process in the first eruption indicated a weakening and partial removal of an overlying magnetic field constraint on the two other filaments, and thus one can physically connect these eruptions as sympathetic. It appears that the peculiar magnetic field configuration in our event was largely favorable to the occurrence of sympathetic filament eruptions. Because coronal dimmings are frequent and common phenomena in solar eruptions, especially in CME events, it is very likely that they represent a universal agent that can link consecutive eruptions nearby with sympathetic eruptions.

Key words: Sun: activity – Sun: coronal mass ejections (CMEs) – Sun: filaments, prominences – Sun: flares – Sun: magnetic topology

1. INTRODUCTION

As a key low-corona signature of coronal mass ejections (CMEs), coronal dimmings have been extensively studied by using observations from the *Yohkoh* Soft X-ray Telescope, the *Solar and Heliospheric Observatory* (*SOHO*), and the *Transition Region and Coronal Explorer* (*TRACE*) in the past decade (for a review, see Hudson & Cliver 2001). They are often associated with eruptions of filament and sigmoidal structures and can take varying forms (Thompson et al. 1998; Zarro et al. 1999 and references therein). Because the typical formation timescale, less than an hour, is much shorter than the typical radiative cooling timescale, about 36 hr, in the corona (Hudson et al. 1996), coronal dimmings are often interpreted as a consequence of density depletions rather than temperature decreases.

It is believed that coronal dimmings are caused first by the expansion of the coronal magnetic field and later by the subsequent mass deletion. Therefore, dimming regions could mark the footprints of the expanding field, and the configuration of dimmings could reflect that of the large-scale magnetic field involved in the associated CME eruptions. Previous observations have shown that the spatial distribution of dimmings might have a complicated pattern (Attrill et al. 2010) and a wide range of scales, from very small (Mandrini et al. 2005; Ren et al. 2008; Innes et al. 2010; Podladchikova et al. 2010; Schrijver 2010) to very large (Wang et al. 2002; Chertok & Grechnev 2005; Zhukov & Veselovsky 2007). Several mechanisms have been proposed to explain the dimming origin. For example, double or core dimmings, a pair of compact and symmetric dimmings within the bend of the magnetic polarity inversion line in the small-scale eruptive source region, were believed to represent the evacuated footprints of a large-scale flux rope ejection (Sterling & Hudson 1997; Webb et al. 2000; Mandrini et al. 2005; Jiang et al. 2007), while remote dimmings associated with brightenings far from the CME source region were considered to be signatures of the expansion of overlying large-scale magnetic fields forced by an erupting flux rope and the interaction between them (Manoharan et al. 1996). On the other hand, widespread secondary dimmings, which are often associated with major flares and powerful CMEs, might involve the eruption of several magnetic flux systems distributed on a large spatial scale. These have been suggested to be produced by a reconnection between the erupting field and the surrounding structures (Attrill et al. 2007, 2009; Mandrini et al. 2007), or by intercoupling and interaction of multiple flux loop systems (Delannée et al. 2007; Zhang et al. 2007; Yang et al. 2011).

The large-scale nature of CMEs raises two universal questions: is there a large-scale reorganization of the coronal magnetic field during the CME? If so, how does it affect the magnetic topology and stability of nearby magnetic structures? Coronal dimmings can be regarded as a good proxy of the relaxation and restructuring of pre-CME closed-field configurations due to the stretching, expanding, or even opening of magnetic field lines; thus, the dimming process should provide crucial information for answering this question. Previous observations speculated that a transient coronal hole, indicating a major reconfiguration of the global magnetic field, might destabilize the neighboring filament and result in its eruption (Watanabe et al. 1992; Srivastava et al. 2000), but details of such a reconfiguration and its function still remain unclear. Mandrini et al. (2007) suggested that dimming regions on the 2003 October 28 CME event could be produced by reconnections between the expanding CME and various magnetic structures, including a magnetic arcade straddling a filament (see their Figure 7), but they did not show whether the filament was disturbed. More recently, Liu et al. (2009) showed that an extended coronal dimming on the 2005 September 13 event might represent partial removal of overlying magnetic fields and relate to a following eruption, but their

event was observed along a single neutral line in the same active region (AR). More studies are needed to clarify the role of coronal dimmings in destabilizing nearby magnetic structures, and detailed observations will provide clues to understand not only the origin of dimmings but also the magnetic topology involved in CMEs.

On 2003 November 19, three filaments erupted successively from different locations on the solar disk in less than 5 hr. Although each eruption was accompanied by a flare, only the first eruption was associated with a CME observed by the Large Angle and Spectrometric Coronagraphs (LASCO) aboard *SOHO*. In particular, coronal dimming regions formed during the first eruption and extended to two neighboring filaments that erupted. In this paper, we present observations of these eruptions and the formation process of the dimmings, as well as a comparison with the coronal magnetic field configuration computed by using the potential-field source-surface (PFSS) model from Schrijver & DeRosa (2003). This enables us to investigate the possible causal linkage of these eruptions and the role of coronal dimmings in their sympathy.

2. OBSERVATIONS

The three eruptions were covered fairly well by the observations at Kanzelhöhe Solar Observatory (KSO) in Austria. We used full-disk Hα line-center images with a pixel size of about 2.″2 and a 1-minute cadence, recorded by a 1k × 1k 10-bit charge-coupled device (Otruba & Pötzi 2003). The first eruption and neighboring dimmings were partially covered by the observations from *TRACE* (Handy et al. 1999), which provided EUV 171 Å images with a pixel size of 0.″5 and a varying cadence. The other two eruptions and extended dimmings were beyond the limited field of view (FOV) of *TRACE* but can be seen in full-disk EUV images from the Extreme Ultraviolet Imaging Telescope (EIT; Delaboudinière et al. 1995) on *SOHO*. The EIT provided 12-minute-cadence 195 Å images with a pixel resolution of 2.″6 of these eruptions. The CME and magnetic field settings in the eruptive regions were examined using *SOHO*/LASCO C2 and C3 data (Brueckner et al. 1995), CME height-time data available on the LASCO Web site, and full-disk magnetograms with a pixel size of 2″ from the Michelson Doppler Imager (MDI; Scherrer et al. 1995) on *SOHO*. Finally, we used the *Geostationary Operational Environmental Satellite (GOES)* soft X-ray light curves to track the times of the associated flares.

3. RESULTS

3.1. General Appearance of the Three Eruptive Filaments

Figure 1 presents general appearances of the three filaments, "F1," "F2," and "F3," before and after their eruptions. We see that F1–F3 were clearly visible in the first Hα image but nearly disappeared in the second image. When we superimposed their pre-eruptive outlines on the corresponding MDI magnetogram, it became clear that they were located along different neutral lines. The first eruption was from F1, a small AR filament that lay along the western boundary of AR10501 (N03° E05°) and was centered at a position angle (P.A.) of about 320°. Note that the AR was near its central meridian passage on November 19. The second eruption originated from F2, a larger quiescent filament along a neutral line to the north of AR10501. It consisted of two sections (indicated by two arrows), had a P.A. of 19°, and was 0.25 $R_\odot$ from F1. F3 was a smaller quiescent filament to the northwest of F1, had a P.A. of about 296°, and was about 0.58 $R_\odot$ from the F1 centroid.

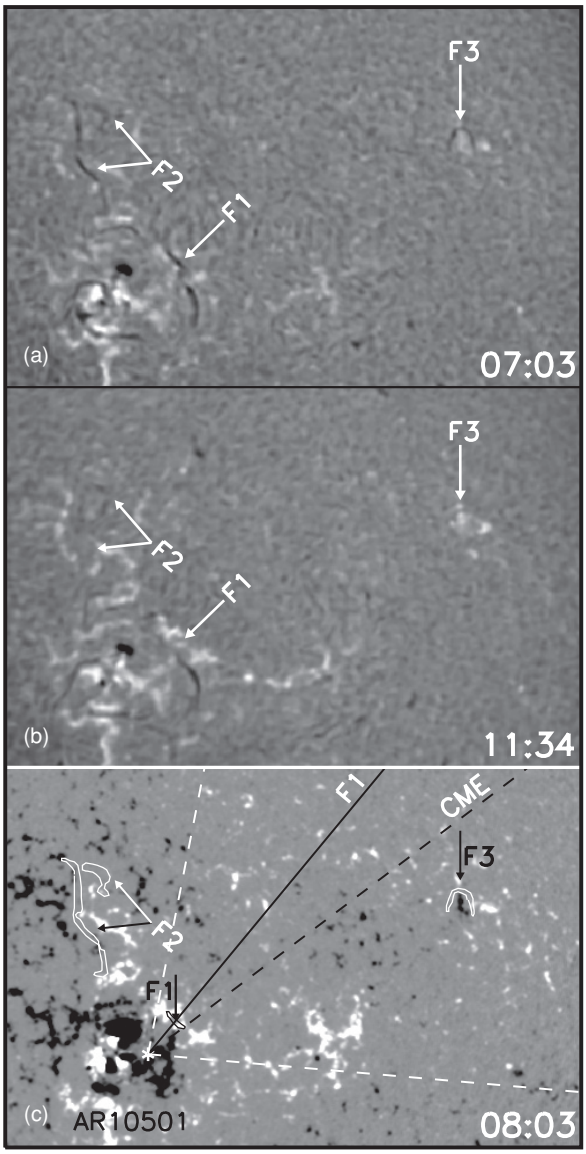

Figure 1. KSO Hα images showing the disappearance of the three filaments, "F1–F3," before (a) and after (b) their eruptions. (c) MDI magnetogram with superposition of F1–F3 outlines determined from the 07:03 UT Hα image shown as white and black contours, showing these filaments approximately dividing the opposite-polarity magnetic fields in the photosphere. The asterisk marks the solar center. The F1 radial (black solid line) and final CME (black dashed line) directions are plotted, and the CME angular size is included between the two white dashed lines. The field of view (FOV) is 1000″ × 660″.

Only the F1 eruption was associated with a CME, with a central P.A. of 307° and a width of 84°. In Figure 1, the final CME direction determined from the central P.A. is plotted by a black dashed line, while the CME angular size determined from its width is subtended by the two white dashed lines. The radial direction of F1, shown by a straight line connecting its centroid to the center of the solar disk, is plotted by a black solid line. We observe that the F1 radial direction had an angle difference of 13° from that of the CME but fell into its angular extent.

3.2. The First Eruption and Dimming Formation

The F1 eruption was followed by a flare of X-ray class C8.8, "FL1," with start, peak, and end times around 07:59, 08:17, and 08:49 UT, respectively. Figure 2 shows a close-up view of the flare process in the *TRACE* FOV. FL1 was a typical

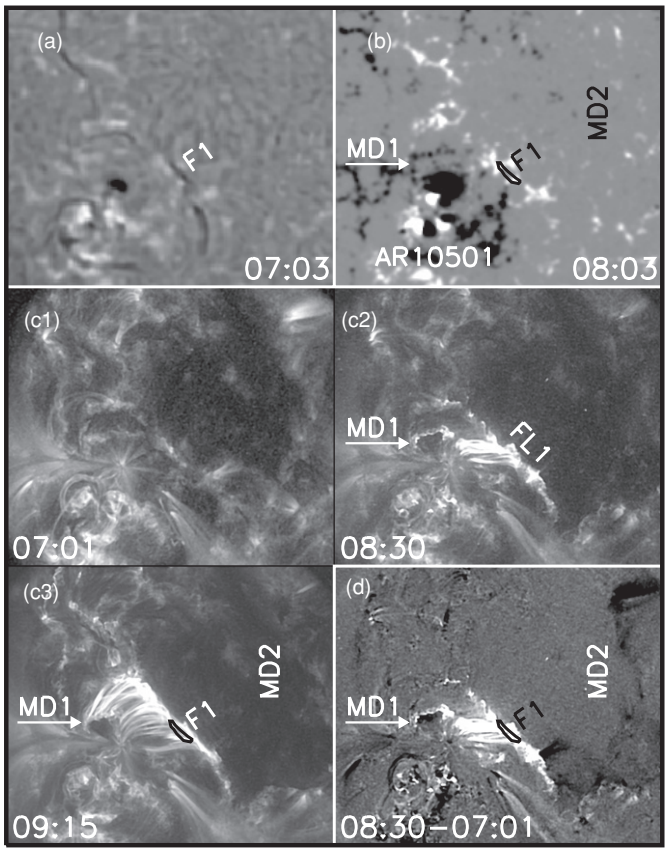

Figure 2. Close-up view of F1 in the KSO Hα image (a), MDI magnetogram (b), and its eruption in *TRACE* 171 Å direct (c1–c3) and fixed-base difference (d) images. The F1 outlines from the 07:03-UT Hα image are superposed as black contours. "FL1" marks the associated flare, and "MD1" and "MD2" mark the two main dimming regions. The FOV is $470'' \times 400''$.

two-ribbon flare, with two ribbons separating from the original F1 on opposite sides and being connected by post-flare loops. As a remarkable characteristic of the eruption, coronal dimmings appeared in the flare course. *TRACE* 171 Å images in Figure 2 clearly show the formation of two main, core dimmings visible near the post-flare arcade (see Attrill & Wills-Davey 2010 and references therein): a compact one, "MD1," in a negative-polarity region immediately adjacent to the main sunspot of AR10501; and a more diffuse one, "MD2," in an opposite-polarity region to the northwest of the eruptive F1. Note that only part of MD2 was seen in the *TRACE* FOV. To examine the overall development and full extent of coronal dimmings due to the F1 eruption and their relationship with the F2 and F3 eruptions, Figure 3 presents KSO Hα and EIT 195 Å observations with a larger FOV.

KSO Hα images show that, consistent with the result of Kalher et al. (1988), F1 was activated before the FL1 start time. At 07:42 UT, F1 was invisible due to brightenings, which obscured its appearance. Another notable characteristic of the F1 eruption is that FL1 was accompanied by the occurrence of two weak, remote brightenings, labeled "WB2" and "WB3" to match the following description. They can be clearly seen by comparing the first and third Hα images. Unlike the two FL1 ribbons, WB2 and WB3 showed no measurable increase in separation but simply faded away in place. Since these remote brightenings were not the result of spreading and expansion of the FL1 ribbons, they should have different origins from that of FL1. The F2 eruption certainly followed that of F1, though its exact start time is difficult to determine. After the maximum time of FL1 (08:17 UT), F2 gradually became ambiguous at Hα. Afterward, brightenings appeared around F2 until it completely disappeared. Ultimately, a flare of X-ray class C4.9, "FL2," took place with start, peak, and end times around 09:26, 09:33, and 09:38 UT, respectively. Note that F2 was invisible at the FL2 start time (09:26 UT). Therefore, it appears plausible that F2 was also activated before its eruption. The F3 eruption occurred about 90 minutes after FL2 ended and was followed by a subflare, "FL3." This will be further discussed later. In summary, the three filament eruptions took place one by one, with long-enough intervals to distinguish them from each other.

In EIT fixed-base difference images shown in Figure 3, the small compact MD1 seen in *TRACE* observations is discernible, while the diffuse MD2 extends to a larger area. Apart from MD1 and MD2, however, two other remote, secondary dimmings (see Mandrini et al. 2007; Attrill et al. 2009 and references therein), "SD3" and "SD4," were also identified in the vicinity of F2 and F3. SD3 surrounded F2, while SD4 was located around F3. Note that the secondary dimmings were well separated from the main dimmings. It is also clear that all dimmings formed in the course of the F1 eruption but persisted throughout the F2 and F3 eruptions. By comparison with MDI magnetograms, we find that MD2 and SD4 corresponded to positive-polarity regions, while MD1 and SD3 corresponded to opposite-polarity regions. Interestingly, when the outlines of WB2 and WB3, determined from the 08:17 UT Hα image, are superimposed on the 08:24 UT EIT 195 Å image, we find WB2 and WB3 to be located at the boundaries of MD2 and SD3, respectively. This is consistent with previous observations that remote brightenings and dimmings can be interrelated phenomena, suggesting that their formation might involve large-scale magnetic reconnection (Manoharan et al. 1996; Jiang et al. 2006; Liu et al. 2006).

3.3. The Second and Third Eruptions

The second eruption showed a complex configuration. F2 consisted of two segments, FL2 included patchy flare brightenings, and SD3 also had a complicated appearance (see Figure 3). To understand the possible interrelationship among F2, FL2, and the surrounding dimming, it is necessary to make a morphological comparison between them. Figure 4 presents a close-up view of the F2 eruptive region. We first see that the two F2 sections became invisible at the maximum time of FL2 at 09:33 UT, meaning that both of them might have erupted. Second, FL2 had three patches of brightenings. They were located on opposite-polarity sides of the two F2 sections: a positive-polarity brightening, "RP," and two negative-polarity ones, "RN1" and "RN2." Therefore, FL2 can still be regarded as a two-ribbon flare, a type often associated with filament eruptions. Finally, SD3 was located in a negative-polarity region around the eruptive F2, without the nearby appearance of opposite-polarity dimming. It is thus reasonable to speculate that, if SD3 corresponds to the negative-polarity footprints of expanding magnetic loop systems, it should have an opposite-polarity counterpart. Clearly, this possibility needs to be clarified further.

Similar to the F2 eruption, the exact start time of the F3 eruption is unknown due to lack of Hα off-band observations, but it definitely took place after the F2 eruption. In Figure 5, the detailed process of the F3 eruption and its association with SD4 are shown in Hα and EIT 195 Å direct images. After the first eruption, F3 underwent some morphological changes at Hα but still persisted in dividing the opposite polarities in the photosphere (see the 10:20 UT image). Its eventual eruption

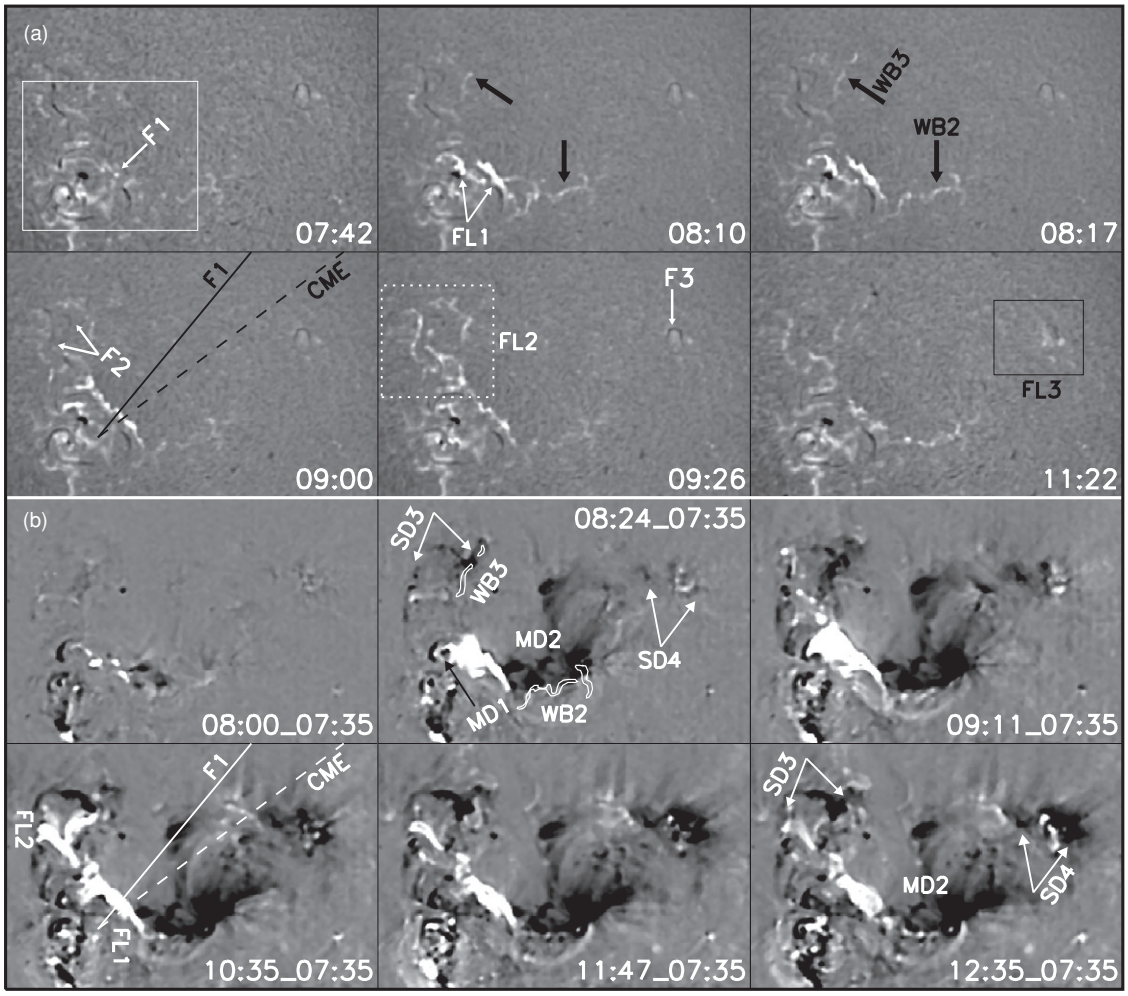

Figure 3. (a) KSO Hα and (b) EIT 195 Å fixed-base difference images showing the three filament eruptions with the same FOV as in Figure 1. "FL1–FL3" mark the three associated flares; "MD1–MD2"/"SD3–SD4" mark the main/secondary dimmings formed in the first eruption; and "WB2" and "WB3," indicated by the black arrows, mark the two remote, weak brightenings. The outlines of WB2 and WB3 from the 08:17-UT Hα image are superposed as white contours in the 08:24-UT EIT image, and the F1 radial and final CME directions are plotted as in Figure 1. The white solid, white dashed, and black solid boxes indicate the FOVs in Figures 2, 4, and 5, respectively.

took place after about 11:10 UT, which led to the subflare FL3, with two ribbons residing on its opposite sides (indicated by the two arrows in the 11:58-UT image). Taking the FL2 end time at 09:38 UT as a reference, it is clear that this eruption was preceded by that of F2. Note that, around the time of the eruption, *GOES* recorded a flare of X-ray class C2.8 between 11:46 and 12:43 UT occurring to the south of AR10501. This was far from FL3, and thus irrelevant to FL3. In EIT 195 Å direct images, the small secondary SD4, formed in the course of the F1 eruption, was immediately adjacent to the eruptive F3 (see the 10:23-UT image) and located in a positive-polarity region. It persisted throughout the F3 eruption but suffered some changes (see the 12:47 UT image). The long-standing maintenance and the close spatial relationship with F3 make us believe that SD4 would exert an effect on the stability of F3 and remain associated with its eruption.

In Figure 6, the light curves of Hα intensities in WB2, WB3, and FL3, as well as EIT 195 Å intensities in the main and secondary dimmings, are plotted and compared with the *GOES-10* 1–8 Å soft X-ray flux and the CME height–time measurements. Using the first-order polynomial fitting, the extrapolated CME onset time is indicated, and the average speed and acceleration of the CME fronts are also shown. It is clear that the 195 Å intensities in MD2, SD3, and SD4 decreased just after the FL1 start time (07:59 UT). The decrease persisted through the extrapolated CME onset time at 08:41 UT. In particular, the increase in Hα intensities in WB2 and WB3 was nearly simultaneous with the decrease in MD2 and SD3 195 Å intensities, respectively. Although the 195 Å intensities in MD1 showed a minor decrease or even increase during and after FL1, possibly due to the extension of the FL1 flare ribbon, there was still an overall decreasing trend. This strongly suggests that the F1 eruption was closely related to the CME and the formation of these dimmings. Note that the maximum time of FL3 (11:33 UT), indicated by its Hα intensity profile, was about 25 minutes earlier than that of the *GOES* C2.8 flare (11:58 UT), though they were close in time. The *GOES* soft X-ray flux of FL3 was below the X-ray class B1 level, and thus *GOES* did not register it as a flare. Moreover, no corresponding optical flare was reported by the online Solar Geophysical Data, possibly because its Hα enhancement was too weak to be regarded as an Hα flare.

4. DISCUSSION

The observations described above reveal the following: the F1 eruption first led to the expanding or even opening of some overlying magnetic loop systems, with footprints manifested by coronal dimmings. Then, the restraining condition of the

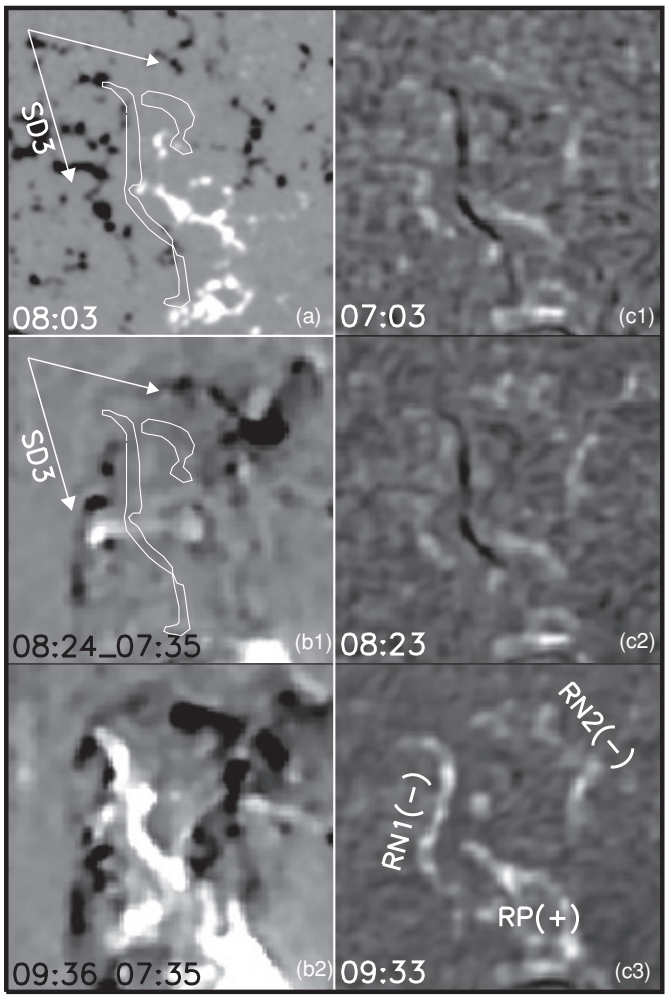

Figure 4. Close-up view of F2 in the MDI magnetogram (a) and KSO Hα image (c1–c2); the surrounding secondary dimming, "SD3," in the EIT 195 Å fixed-base difference image (b1–b2); and FL2 in the Hα image (c3). The F2 outlines from the 07:03-UT Hα image are superposed as white contours. "RP," "RN1," and "RN2" mark the three flaring patches of FL2, and the plus/minus signs mark the corresponding magnetic polarities in the photosphere. The FOV is $300'' \times 300''$.

magnetic loop systems on F2 and F3 was altered or partially removed, thus affecting their stability to such an extent that they could completely erupt. If this is true, the magnetic connectivity of the dimmings should contain the key elements that are needed to produce the F2 and F3 eruptions, and the knowledge of a large-scale configuration is crucial for an understanding of a causal link between these successive eruptions. Using the PFSS software package available in SolarSoftWare that is based on synoptic magnetic maps from MDI with a 6 hr time resolution, in Figure 7 we present the result of the magnetic field line extrapolation performed by Schrijver & DeRosa (2003; see Schrijver & DeRosa 2003 for a detailed description of the procedure). We use the synoptic map at the time close to the event studied here, and only the magnetic field lines that overlie the eruptive filaments and have one or two footprints in the dimmings are selected. The outlines of the three filaments (red), the two remote brightenings (white), and the final CME (white) and F1 radial (pink) directions are also superposed. There are multiple magnetic arcades and loop systems in this configuration. In addition to three confined arcades (orange), "a1," "a2," and "a3," holding F1, F2, and F3, respectively, we can distinguish four other extended loop systems, labeled "L1," "L2," "L3," and "L4," in terms of the magnetic field line connectivity between the dimmings. L1 (blue) is an extended loop system overlying F1 and connecting major parts of MD2 to a confined region around MD1. L2 (green) is a more extended loop system overlying F2. Clearly, its positive-polarity footprints anchor a region near SD4, while the negative-polarity footprints are located around SD3. L3 (pink) does not contain any filament but connects SD3 to a region north of MD2. L4 (red) is a far-reaching loop with a negative-polarity footprint near MD1 and an opposite-polarity one in SD4.

Although the three flares might be relevant to the openings and closing reconnections of the three confined arcades driven by the eruptive filaments, it is quite probable that the dimmings are mainly caused by the expansion of the four extended loop systems. According to the magnetic connectivity and magnetic setting at its feet, we speculate that the dimming formation might involve two processes. First, simple expansion and eruption of L1, L2, and L4, pushed outward by the erupting F1 along the CME direction, would produce MD1 and major parts of MD2, SD3, and SD4. As a result, the restrictions of L2 on F2 and L4 on F3 would be weakened and smoothen their eruptions. As a component of the CME, therefore, the expansion of these loop systems might be directly related to the instabilities of F2 and F3. Second, consistent with the new CME evolution model recently proposed by Attrill et al. (2007), the lateral expansion of the erupting L1 would drive magnetic reconnection with L3 and lead to the partial formation of MD2 and SD3. In particular, WB2 and WB3 along the boundaries of MD2 and SD3 might be a creditable signature of such reconnection. It is noteworthy that, if the erupting L1 occurs along the CME direction and the CME angular size (subtended by the two dashed white lines in Figure 7) can reflect its lateral expansion, L1 would encounter L3 in an orientation that would favor a forced reconnection. In such a case, it is clear that the dimming formation would not directly make an impact on the stabilities of F2 and F3 because L1 and L3 do not cover the two filaments. However, the erupting L1 could undergo similar reconnection with a3. This also would be responsible for the partial formation of SD4, reduce magnetic tension of a3, and relate to the F3 eruption. A previous example given by Mandrini et al. (2007) showed that reconnections between an expanding CME and a magnetic arcade over a filament might lead to the formation of nearby coronal dimmings.

Therefore, at least a portion of these dimmings in our case can be taken as an indicator of the removal of the magnetic field barriers overlying F2 and F3, so long as the dimmings represent the feet of the expanding loop systems. As a result, the entire eruption series, which showed close continuity, was joined together by the dimming formation from the first eruption. Such a situation reminds us of so-called sympathetic eruptions that consecutively occur in different locations and have certain physical connections (Pearce & Harrison 1990; Moon et al. 2002, 2003; Wheatland & Craig 2006). In this sense, we call the eruptions in our event "sympathetic filament eruptions" since they occurred along separate neutral lines. Different from previously found varied agents linking sympathetic flares (Shi et al. 1997; Gopalswamy et al. 1999; Bagala et al. 2000; Zhang et al. 2000; Wang et al. 2001; Jiang et al. 2008, 2009a), our observations suggest, for the first time, that coronal dimmings can also act as an agent that connects sequential filament eruptions from different arcades to sympathetic ones.

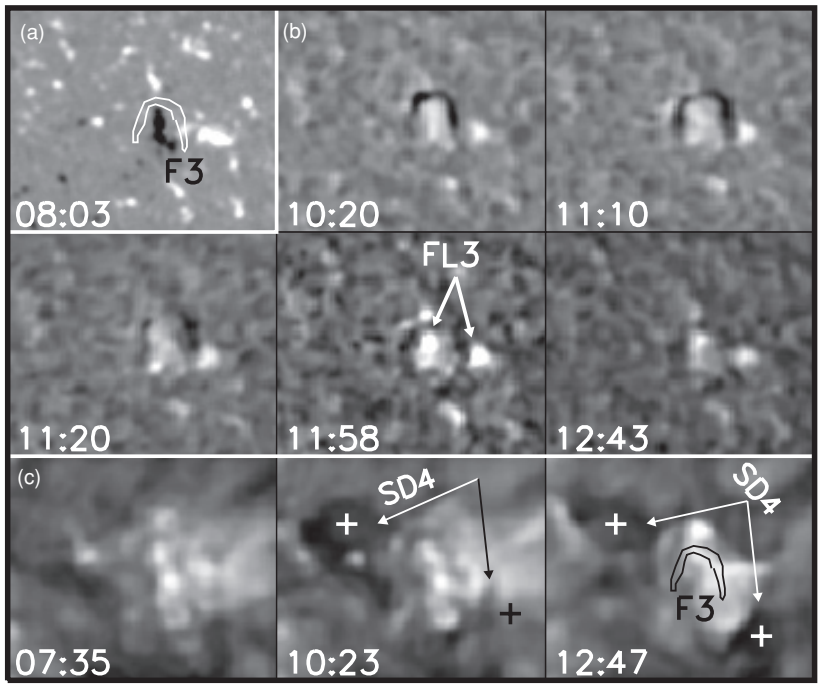

Figure 5. Close-up view of F3 in the MDI magnetogram (a), its eruption in KSO Hα images (b), and the surrounding secondary dimming, "SD4," in EIT 195 Å direct images (c). The F3 outlines from the 07:03 UT Hα image are superposed as white and black contours, the thick white arrows indicate the two ribbons of FL3, and the plus signs mark the corresponding magnetic polarity in the photosphere. The FOV is $240'' \times 200''$.

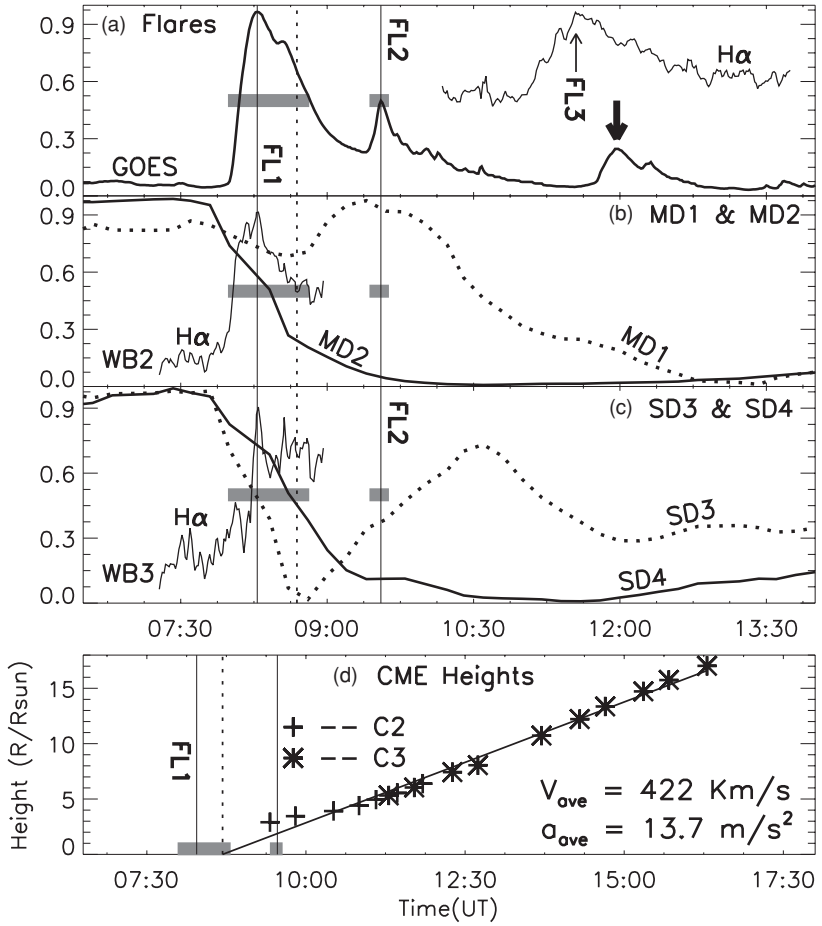

Figure 6. Time profiles of the *GOES-10* 1–8 Å soft X-ray flux (thick solid line in (a)); the light curves of KSO Hα intensities in FL3, WB2, and WB3 (thin solid lines in (a)–(c)); and EIT 195 Å intensities in the dimming regions (dashed and thick solid lines in (b) and (c)) as a function of time. (d) Heights of the CME fronts as a function of time and the back-extrapolations via the use of the first-order polynomial fitting. The vertical solid bars indicate the peak times of FL1 and FL2, the dashed bars indicate the extrapolated onset time of the CME, and the horizontal bars indicate the durations of FL1 and FL2. The thin arrow indicates the FL3 peak time at Hα, and the thick arrow indicates a *GOES* C2.2 flare close in time to FL3.

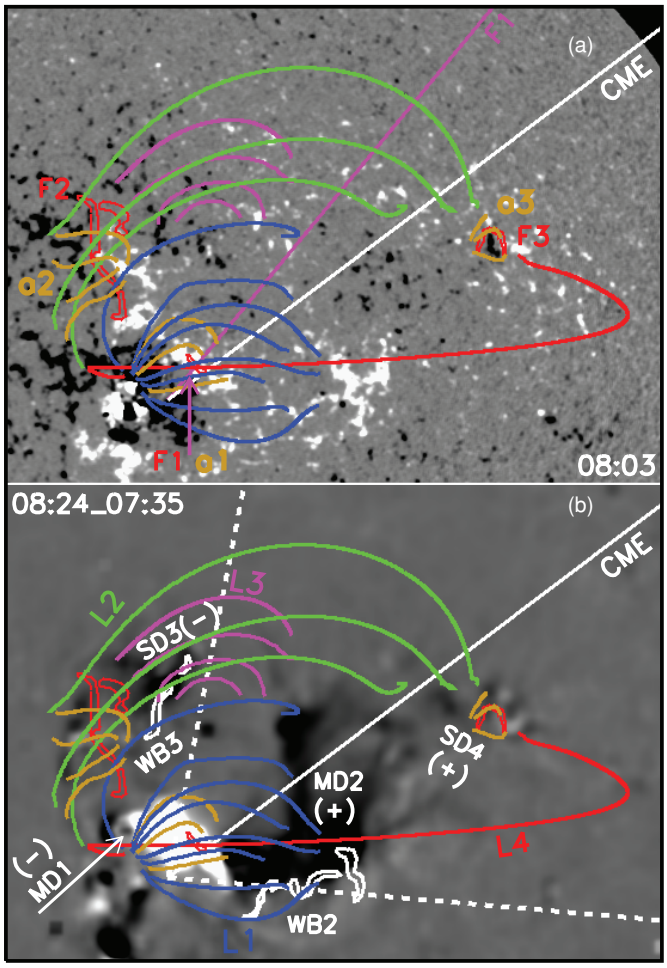

Figure 7. Overlay of the MDI magnetogram (a) and EIT 195 Å fixed-base difference image (b), with the extrapolated field lines emphasizing the magnetic connectivity between the dimming regions. The outlines of WB2 and WB3 (white) and F1–F3 (red) are overlaid, the F1 radial (pink) and final CME (white) directions are plotted, and the angle included between the two dashed white lines indicates the CME's angular size. Four distinct loop systems, "L1" (blue), "L2" (green), "L3" (pink), and "L4"(red), are anchored in or around the dimming regions, and three arcades, "a1," "a2," and "a3" (orange), straddle F1–F3, respectively. The FOV is $1100'' \times 800''$.

The key to sympathetic filament eruptions is the physical connection between eruptions. It is reasonable to imagine that such a connection can be established by an earlier eruption that decreased the magnetic fields overlying other nearby filaments. Such a possibility has already been considered by some previous observational and theoretical studies. Webb et al. (1997) showed that several distinct phases or separate eruptions may have occurred consecutively at different positions under multiple arcades, and suggested that the interplay or interaction between different arcades is fundamental to the eruption process. In the framework of the magnetic breakout model (Antiochos et al. 1999) with a quadrupolar configuration, an erupting, low-lying core magnetic field can reconnect with an oppositely directed, overlying background bipolar field. Observations of Gary & Moore (2004) revealed that a central breakout (the first filament eruption) can remove overlying magnetic loops, produce a weakened field configuration, and then lead to a lateral breakout (the second filament eruption). Wang et al. (2006) found that activation and eruption of a huge transequatorial filament appeared to be an essential part of a subsequent filament eruption and flare. The MHD models of Ding et al. (2006) and Peng & Hu (2007) also suggested that the interaction between different magnetic flux systems may serve as a possible mechanism for sympathetic events. Nagashima et al. (2007) suggested that small flares can change overlying magnetic topology via small-scale reconnection and eventually lead to a nearby catastrophic filament eruption. Jiang et al. (2009b) recently provided further observational evidence of the arcade interaction that resulted from a filament eruption. In particular, Zuccarello et al. (2009) posited a so-called domino effect: an initial filament eruption would trigger a sequence of phenomena, ultimately causing a reduction in the magnetic tension of higher arcades such that other nearby filaments were free to erupt. Therefore, our event supports the focus of these previous works: that, as an exterior driving mechanism, the weakening and partial removal of the overlying magnetic field restraint might play an important role in filament eruptions. This is clearly different from other exterior agents of filament instability, for example, flux emergences and cancellations in or adjacent to filament channels. Our observations go a step further to show that the dimming formation in one eruption might be a key proxy for the relaxation of magnetic configurations (Mandrini et al. 2007; Liu et al. 2009) that can lead to other interdependent eruptions.

Because of the high temporal closeness of the three filament eruptions, we pay special attention to the role of the coronal dimmings in the F2 and F3 eruptions; otherwise, these successive eruptions could be considered unrelated events. Since coronal dimmings are frequently observed during solar eruptions, we expect that successive eruptions connected by dimmings should be common phenomena. There are two reasons why previous observations missed similar eruptions and their link. First, the main interest of many studies was focused on eruptions that resulted in dimmings and CMEs. Second, a late eruption might be neglected due to its unimpressive appearance in low-resolution EIT observations, its large spatial scale that exceeds the limited *TRACE* FOV, and the lack of dimming signals in ground-based Hα images. Obviously, the possibility of coronal dimmings acting as causal links between sympathetic eruptions calls for a detailed verification via further observational and theoretical works. It is anticipated that observations from the *Solar Terrestrial Relations Observatory* (*STEREO*) and the *Solar Dynamics Observatory* (*SDO*) will be beneficial.

5. SUMMARY

We present the first observational evidence that coronal dimmings can link consecutive filament eruptions from different locations as sympathetic, provided that they represent the feet of expanding magnetic loop systems. The three filament eruptions we examined, which occurred one by one in less than 5 hr, had a close temporal relationship. During the initial F1 eruption that resulted in a CME, both main and secondary dimmings formed. The secondary dimmings were close to the other two filaments and survived their later eruptions, suggesting that these filament eruptions are interdependent phenomena. The dimmings can be formed in two ways: the simple expansion of flux systems forced by the erupting F1 field, and the interaction or reconnection of the erupting F1 field with ambient magnetic fields, including a magnetic arcade over F3. As a result, the overall field configuration was relaxed and the stabilizing magnetic fields of F2 and F3 were partially destroyed, which eventually led to their eruptions. In our special magnetic configuration, therefore, the coronal dimmings indirectly manifested the weakening and partial removal of the magnetic field constraints on F2 and F3 and connected the three filament eruptions.

Large-scale magnetic topology plays an important role in the new driving mechanism of sympathetic filament eruptions. In particular, our observations strongly suggest that, when seemingly irrelevant filament eruptions successively occur in the vicinity of coronal dimmings produced by a preceding eruption, they might be interdependent and should be examined on a case-by-case basis with great caution. In a similar event, it will be significantly helpful to determine the peculiar large-scale magnetic configuration, for example, by using the convenient PFSS computational results of Schrijver & DeRosa (2003). More observations are needed to further detail this mechanism.

We thank an anonymous referee for many constructive suggestions and thoughtful comments that improved the quality of this paper. We are grateful to the observing staff at KSO for providing Hα data. We also thank the *GOES*, *TRACE*, *SOHO*/EIT, LASCO, and MDI teams for data support. This work is supported by the 973 Program (2011CB811403), by the Natural Science Foundation of China under grants 10973038 and 40636031, and by the Scientific Application Foundation of Yunnan Province under grants 2007A112M and 2007A115M.

REFERENCES

Antiochos, S. K., DeVore, C. R., & Klimchuck, J. A. 1999, ApJ, 510, 485
Attrill, G. D. R., Engell, A. J., Wills-Davey, M. J., Grigis, P., & Testa, P. 2009, ApJ, 704, 1296
Attrill, G. D. R., Harra, L. K., van Driel-Gesztelyi, L., & Démoulin, P. 2007, ApJ, 656, L101
Attrill, G. D. R., & Wills-Davey, M. J. 2010, Sol. Phys., 262, 461
Bagala, L. G., Mandrini, C. H., Rovira, M. G., & Démoulin, P. 2000, A&A, 363, 779
Brueckner, G. E., Howard, R. A., Koomen, M. J., et al. 1995, Sol. Phys., 162, 357
Chertok, I. M., & Grechnev, V. N. 2005, Sol. Phys., 229, 95
Delaboudinière, J.-P., Artzner, G. E., Brunaud, J., et al. 1995, Sol. Phys., 162, 291
Delannée, C., Hochedez, J.-F., & Aulanier, G. 2007, A&A, 465, 603
Ding, J. Y., Hu, Y. Q., & Wang, J. X. 2006, Sol. Phys., 235, 223
Gary, G. A., & Moore, R. L. 2004, ApJ, 611, 545
Gopalswamy, N., Nitta, N., Manoharan, P. K., Raoult, A., & Pick, M. 1999, A&A, 347, 684
Handy, B. N., Acton, L. W., Kankelborg, C. C., et al. 1999, Sol. Phys., 187, 229
Hudson, H. S., Acton, L. W., & Freeland, S. L. 1996, ApJ, 470, 629
Hudson, H. S., & Cliver, E. W. 2001, J. Geophys. Res., 106, 25199
Innes, D. E., McIntosh, S. W., & Pietarila, A. 2010, A&A, 517, L7
Jiang, Y., Bi, Y., Yang, J., Zheng, R., & Wang, J. 2009a, Res. Astron. Astrophys., 5, 603
Jiang, Y., Li, L., Zhao, S., et al. 2006, New Astron., 11, 612
Jiang, Y., Shen, Y., Bi, Y., Yang, J., & Wang, J. 2008, ApJ, 677, 699
Jiang, Y., Yang, J., Zheng, R., Bi, Y., & Yang, X. 2009b, ApJ, 693, 1851
Jiang, Y., Yang, L., Li, K., & Shen, Y. 2007, ApJ, 662, L131
Kahler, S. W., Moore, R. L., Kane, S. R., & Zirin, H. 1988, ApJ, 328, 824
Liu, C., Lee, J., Deng, N., Gary, D. E., & Wang, H. 2006, ApJ, 642, 1205
Liu, C., Lee, J., Karlický, M., et al. 2009, ApJ, 703, 757
Mandrini, C. H., Nakwacki, M. S., Attrill, G. D. R., et al. 2007, Sol. Phys., 244, 25
Mandrini, C. H., Pohjolainen, S., Dasso, S., et al. 2005, A&A, 434, 725
Manoharan, P. K., van Driel-Gesztelyi, L., Pick, M., & Demoulin, P. 1996, ApJ, 468, L73
Moon, Y.-J., Choe, G. S., Park, Y. D., et al. 2002, ApJ, 574, 434
Moon, Y.-J., Choe, G. S., Wang, H., & Park, Y. D. 2003, ApJ, 588, 1176
Nagashima, K., Isobe, H., Yokoyama, T., et al. 2007, ApJ, 668, 533
Otruba, W., & Pötzi, W. 2003, Hvar Obs. Bull., 27, 189
Pearce, G., & Harrison, R. A. 1990, A&A, 228, 513
Peng, Z., & Hu, Y. Q. 2007, ApJ, 668, 513
Podladchikova, O., Vourlidas, A., Van der Linden, R. A. M., Wülser, J.-P., & Patsourakos, S. 2010, ApJ, 709, 369
Ren, D., Jiang, Y., Yang, J., et al. 2008, Ap&SS, 318, 141
Scherrer, P. H., Bogart, R. S., Bush, R. I., et al. 1995, Sol. Phys., 162, 129
Schrijver, C. J. 2010, ApJ, 710, 1480
Schrijver, C. J., & DeRosa, M. L. 2003, Sol. Phys., 212, 165
Shi, Z.-X., Wang, J.-X., & Luan, D. 1997, Acta Astron. Sin., 38, 257
Srivastava, N., Schwenn, R., Inhester, B., Martin, S. F., & Hanaoka, Y. 2000, ApJ, 534, 468
Sterling, A. C., & Hudson, H. S. 1997, ApJ, 491, L55
Thompson, B. J., Plunkett, S. P., Gurman, J. B., et al. 1998, Geophys. Res. Lett., 25, 2465
Wang, H., Chae, J., Yurchyshyn, V., et al. 2001, ApJ, 559, 1171
Wang, J., Zhou, G., Wen, Y., et al. 2006, Chinese J. Astron. Astrophys., 6, 247
Wang, T., Yan, Y., Wang, J., Kurokawa, H., & Shibata, K. 2002, ApJ, 572, 580
Watanabe, T., Kozuka, Y., Ohyama, M., et al. 1992, PASJ, 44, L199
Webb, D. F., Kahler, S. W., McIntosh, P. S., & Klimchuck, J. A. 1997, J. Geophys. Res., 102, 24161
Webb, D. F., Lepping, R. P., Burlaga, L. F., et al. 2000, J. Geophys. Res., 105, 27251
Wheatland, M. S., & Craig, I. J. D. 2006, Sol. Phys., 238, 73
Yang, J., Jiang, Y., Zheng, R., et al. 2011, Sol. Phys., 270, 551
Zarro, D. M., Sterling, A. C., Thompson, B. J., Hudson, H. S., & Nitta, N. 1999, ApJ, 520, L139
Zhang, C., Wang, H., Wang, J., et al. 2000, Sol. Phys., 195, 135
Zhang, Y., Wang, J., Attrill, G. D. R., et al. 2007, Sol. Phys., 241, 329
Zhukov, A. N., & Veselovsky, I. S. 2007, ApJ, 664, L131
Zuccarello, F., Romano, P., Farnik, F., et al. 2009, A&A, 493, 629